Exploitation of industrial solid wastes for preparing zeolite as a value-added product and its kinetics as adsorbent for heavy metal ions

R.M. Abdel-Hameed [1], **F.E. Farghaly** [1], **E.A. Abdel-Aal** [1], **I.A. Ibrahim** [1], **M.A. Ahmed** [2], **M.F. Abdel-Messih** [2], **M.A. Abdel Khalek** [1]

[1] Central Metallurgical Research and Development Institute (CMRDI), P.O. Box 87 Helwan 11421, Cairo, Egypt

[2] Chemistry Department, Faculty of Science, Ain shams University, Cairo, Egypt

Corresponding author: rehamabdelhamed81@gmail.com (R.M. Abdel-Hameed)

Abstract: Aluminum and fumed silica as solid industrial wastes were converted to zeolite NaP as a value-added product without any template. The hydrothermal process was optimized using static autoclave. The crystallization was carried out at 100, 120 and 150°C for 24, 48 and 72 h. The prepared zeolite of Si:Al ratio of 1.2 was characterized using X-ray Diffraction (XRD), Scanning Electron Microscope (SEM) provided with Energy Dispersive Spectroscopy (EDS), Surface Area, Fourier Transmitted Infra-Red (FTIR) and Thermal Analysis (TG-DSC). The crystalline phase was formed at 100°C after 72 hours and at 120°C after 48 hours, while it was formed after 24 h only at 150°C. Increasing temperature and time lead to the conversion of the prismatic gibbsite crystals into plate-like structure of zeolite which is then formed cauliflower-like structure. The prepared zeolite was employed as adsorbent for Ni^{2+} and Cu^{2+} ions from aqueous solution. The kinetic studies of adsorption processes were performed.

Keywords: zeolite P, aluminum wastes, hydro-thermal process, metal ion removal, aluminum waste

1. Introduction

Aluminum is one of the most commonly used metals in most forms of everyday life. It is produced from bauxite ore in the primary industry and from scraps in the secondary industry (Tsakiridis et al., 2013). Both industries generate wastes as slag or dross. They contain ultra-fine particle size, which is not a marketable product due to its lower aluminum content (Galindo et al., 2015a). Aluminum waste is considered as hazardous waste due to its risk to the environment and to human health (Galindo et al., 2015b). The European Waste Catalogue classifies it as a hazardous waste. The black dross and ball mill dust is highly flammable able to release toxic gases such as ammonia, methane and hydrogen sulfide. The main negative impacts come from its very fine grain size and its heterogeneous chemical composition (Mahinroostaa and Allahverdi, 2018; López-Delgado et al., 2020). The aluminum content (as oxide) in the most aluminum wastes is approximately 53-81% by weight. Also, the amount of silica fume generated from ferrosilicon alloys and silicon metal industries about 1,000,000 tons. About 25,000 tons of silica fume are produced each year by the Egyptian Ferroalloys Co. (EFACO) from its ferrosilicon plant located in the Edfu City (xalinyuan, 2020). So, they must be used as a "secondary" raw material for the production of added-value materials. (López-Delgado and Tayibi, 2012).

Zeolite is microporous, alumino-silicate mineral. Its importance arises from its structure. It has a three-dimensional tetrahedral structure with negative surface charge. It is generated as a result of isomorphous substitution of Si^{4+} by Al^{3+}. It may be balanced by alkali and alkali-metal cations and water molecules. It has a general formula of $M_{2/n}OAl_2O_{3x}SiO_{2y}.H_2O$ where M is alkali or alkaline earth element, n is the valence charge on that element, x varies from 2 to 10 and y varies from 2 to 7 (Corma, 1997; Cundy and Cox, 2005; Moliner et al., 2013; Cejka et al., 2016; Visa, 2016). The flexibility of Si-O-Si bond explains its 200 structure forms (Meftah et al., 2008). Zeolite is characteristic of high surface area,

micro porosity, high ion-exchange capacity and high stability (Larsen, 2007; Garcia, et al., 2016). Thus, it is applied in ion exchange, catalysis, chemical separation and membranes (Cao et al., 2008; Huang, 2010).

It is reported that, the Zeolite could be synthesized by different methods. The most common methods are sol-gel, hydrothermal synthesis and microwave heating synthesis (Zubowa et al., 2008). The hydrothermal method includes also the zeolite crystallization from aqueous systems (Vartuli et al., 2000; Boukadir et al., 2002; Hu and Liu, 2003; Aguado et al., 2004). They are prepared by using organic structure-directing agents (OSDAs) (Lobo et al., 1995). However, there are a limited number of zeolites that can be synthesized by OSDA-free routes (Oleksiak and Rimer, 2014). The OSDA-free crystallization of zeolites is not easy to control (Navrotsky et al., 2009; Maldonado et al., 2013; Oleksiak et al., 2016). Although, all zeolites have the same formula and geometric structure, but the SiAl ratio, Na content and hydration is difficult to determine. This is attributed to high flexible of the SiAl link (Hansen et al., 1993; Meier and Olsen, 1996).

There are three polymorphs of zeolite Na-P: cubic (Na-P1), tetragonal (Na-P2) and more rarely orthorhombic (Na-P3). Na-P1 has been described as a body-centred tetragonal with a unit cell of pseudo-cubic geometry (Baerlocher and Meier, 1972; Gottardi and Galli, 1985; Rodrigues et al., 2016). Gismondine framework of zeolite (GIS) and other framework types have proven to be excellent materials for small liquid or gas molecule separation, the removal of radioactive and toxic waste species from wastewaters, and water softening in detergents (Adams et al., 1997; Huo et al., 2012). Zeolite synthesis occurs at temperatures from 70 to 250°C. Some conditions of extreme importance, such as SiAl ratio, crystallization time and temperature (Delgado et al., 2014).

This work aims to develop the hydrothermal process to prepare zeolite from aluminum and silica fume as waste materials without using any template. Then the produced zeolite will be investigated as absorber for copper and nickel ions from aqueous solutions.

2. Materials and methods

2.1. Materials

Ultra-fine aluminum powder waste is supplied by Alumisr Co., for the aluminum industry, Helwan, Egypt. Silica waste and fumed silica were supplied by ferrosilicon Co., Egypt. The particle size is less than 0.074 mm and they are employed as raw materials for zeolite preparation without further treatment. Sodium hydroxide pellets, as a source of alkali was supplied by Sigma Aldrich. Copper sulfate ($CuSO_4.5H_2O$) and Nickel nitrate ($Ni(NO_3)_2.6H_2O$) of reagent grade, Merck Chemicals GmbH are used for preparation of Cu^{2+} and Ni^{2+} ions solutions.

2.2. Methods

2.2.1. Zeolite synthesis

The calculated amount of sodium hydroxide is dissolved in a small amount of pure water. The solution is divided into two portions. Silica waste is added to the first portion and the aluminum waste is added to the second portion. The two solutions were mixed together for 1 h and left for another 1h for aging. Then, it is transferred to a Teflon-lined autoclave reactor. The product is quenched in water, filtered and washed with distilled water till pH 9 and it is dried at 100°C for 24 h.

2.2.2. Characterization of zeolite

The prepared zeolite are characterized using BRUKER X-Ray Diffractometer (Germany) Model AXS D8 with Cu-target (λ=1.540 Å and n=1) at 40 kV potential and 40 A was used for characterization of the crystal structure of synthesized zeolite. The diffraction data were recorded for 2θ values between 10° and 80° and the scanning rate was 3° min^{-1} or 0.02°/0.4 sec. Micro-pore and BET specific surface area are measured using nitrogen adsorption–desorption isotherms using BEL (Japan) nitrogen adsorption apparatus. A sample is degassed at 120°C prior to BET measurements. The BET specific surface area (SBET) is determined by a multipoint BET method using the adsorption data in the relative pressure P/P0 range of 0.05–0.25. The surface morphology and microstructure of gold coated synthesized zeolite

were identified by JEOL instrument (Japan) model JSM-5410 scanning electron microscope (SEM) at 15 kV of excitation potential. Mattson 1000, series LC operating, issue I (0791) spectro-photometer was used for Fouriertransform infrared (FTIR) measurement in the transmission mode, with a wave number range of 4000-400 cm^{-1}. The spectrum of the sample is carried out in KBr powder using a resolution of 4 cm^{-1}. Standard software (Omic ESP, version 5.1) was used for data acquisition and analysis. The wastes were analyzed using X-Ray Fluorescence, XRF (Axios Advanced WDXRFP analytical, Netherland). Energy Dispersive X-Ray spectroscopy EDX attachment with Bruker AXS-Flash Detector 410-M, Germany, is used for characterization. The atomic absorption AAnalyst 200, was used for elemental analysis of digested sample in 20% hydrofluric acid solution.

2.2.3. Adsorption procedure

An attempt was made to use the zeolite for removal of Ni^{2+} and Cu^{2+} ions aqueous solutions. A 0.05 g of Zeolite is added to 25 ml of synthetic solution and stirred at 200 rpm for different time intervals at the desired pH and temperature.

The removal percent and the sorption capacity of adsorbent were calculated by Eqs. (1) & (2), respectively (Mohora et al., 2012).

$$Removal(\%) = \frac{c_i - c_t}{c_i} \times 100 \tag{1}$$

where C_i and C_t are the ion concentration (mg/l) at time zero and t, respectively.

$$q_e = \frac{(c_i - c_t)V}{M} \tag{2}$$

where q_e is the sorption capacity of adsorbent at time t, (mg/g), V is the solution volume (liter) and M is the adsorbent weight (g).

3. Results and discussion
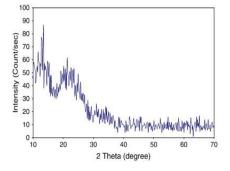
3.1. Characterization of silica and aluminum wastes

XRF of fumed silica shows that it is composed of 96.18% SiO$_2$ with low impurities, Table 1. The relative density of silica fume is 2.14 g/cm^3. XRD indicated that the main phase of silica fume waste is amorphous silicon dioxide. SEM photograph showed that the silica particles are almost spherically agglomerated, Fig. 1. It is composed of fine vitreous particles with a surface area 20 m^2/g.

XRF of aluminium waste (Table 2) shows that it has high aluminum content (Al$_2$O$_3$ = 59%) with SiO$_2$ = 1.36% and Na$_2$O = 2.12%. Also, minor MgO, P$_2$O$_5$, Fe$_2$O$_3$, CuO, ZnO, PbO and SO$_3$ are detected.

The XRD pattern showed that it is mainly composed of gibbsite (aluminum hydroxide) - Fig. 2. FTIR scan confirms the gibbsite composition - Fig. 3 (Rodrigues et al., 2016). Morphology and EDS show hexagonal and prismatic gibbsite crystals with chamfered faces of different sizes (Huo et al., 2012) - Fig. 4.

Table 1. Chemical analysis of the applied silica fume

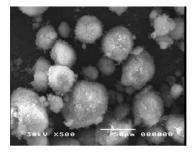| Item	SiO$_2$	CaO	TiO$_2$	K$_2$O	MnO	Al$_2$O$_3$	Fe$_2$O$_3$	P$_2$O$_5$	Na$_2$O	MgO	L.O.I.	Total
%	96.19	0.321	0.003	0.159	0.036	0.511	0.231	0.005	0.012	0.016	2.080	99.56

Fig. 1. XRD pattern and SEM photograph of silica fume

Table 2. Chemical analysis of Alumisr aluminum waste

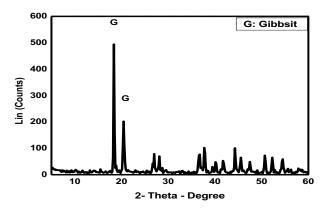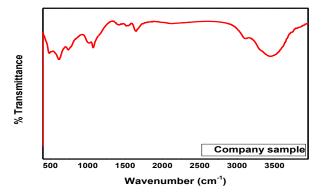| Item	Al$_2$O$_3$	SiO$_2$	Na$_2$O	MgO	P$_2$O$_5$	Fe$_2$O$_3$	CuO	ZnO	PbO	SO$_3$	CaO	L.O.I	Total
%	59.04	1.36	2.12	0.473	0.072	0.717	0.045	0.104	0.013	0.327	1.54	34.17	**99.98**

Fig. 2. XRD pattern of Aluminum waste

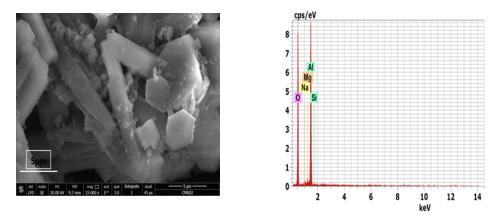Fig. 3. FTIR spectra of Aluminum waste

Fig. 4. SEM and EDX of Aluminum waste

3.2. Zeolite preparation

As stated in latter studies the molar ratio of Si/Al is the most important parameter that controls crystallization and morphology of zeolite (Huo et al., 2012). The most appropriate ratio of Si/Al reported in literature where high-silica, cubic NaP,(Si/Al = 3.38) and NaP2(Si/Al = 4.6) (Larsen, 2007) are required is 1.2. Thus, the preparation is carried out with the most favourable silicon and aluminum ratio (1.2) which obtains the maximum yield. Because the crystal growth and zeolite type depend on the crystallization time and temperature (Mohora et al., 2012), both factors were investigated.

Fig. 5 shows that the NaP zeolite is formed, but with very low crystallinity at crystallization time 72 h, but at 48 h and 24 h the gibbsite is formed with different crystallinity at 100°C, where at 24 h the gibbsite formed with high crystallinity. It means that the low temperature and time are not effective. By increasing the time the gibbsite is formed with less crystallinity, which confirms the nucleation and crystal growth with time. Fig. 6 shows that at 120°C an amorphous phase is formed after 24 h, while the crystalline phase is formed after 48 and 72 h. At 150°C, NaP zeolite which is based on framework type gismondine is formed, Fig. 7. Its crystallinity is increased with increasing crystallization time. The crystallization time 72 h is a suitable for crystalline zeolite NaP formation at all temperatures, Fig. 8. It means that the increasing time up to 72 h, and temperature up to 150°C seems to increase the crystallinity of the zeolite. Increasing temperature decreases the surface area, while it increases the average crystal size, Table 3 (Abdel-Khalek et al., 2019).

Table 3. Effect of temperature on crystallinity, surface area and average crystal size

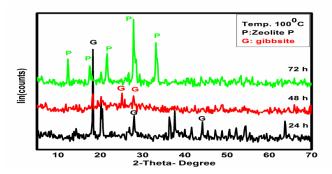| Temperature, °C	Surface area, m^2/g	crystal size, nm	Formed phase
100	176.2	31.6	P2
120	134.8	33.7	P2
150	112.3	39.8	P2

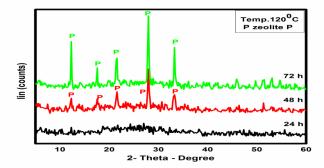Fig. 5. XRD pattern of formed zeolite at 100°C

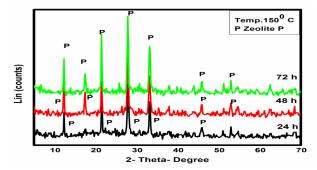Fig. 6. XRD pattern of prepare zeolite at 120°C
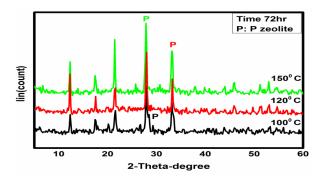

Fig. 7. XRD pattern of prepare zeolite at 150°C

Fig. 8. Effect of temperature on zeolite crystallinity

Fig. 9 shows that the gibbsite crystal of aluminum waste is still after 24 h at 100°C. After 48 h the gibbsite is observed, but with prismatic shape and plates. After 72 h multifaceted shape as that of NaP is formed. At 120°C the amorphous phase is converted to cauliflower-like structure as time increases up to 72 h, Fig. 10. At 150°C for all time, the products have multifaceted shape, Fig. 11. The formed zeolite after 48 h has bigger crystal size than that obtained after 24 h. Several small particles aggregated are noted together without isolation. It is the characteristic morphology of NaP zeolite, which is consist of "cauliflower-like" primary aggregates with well-defined crystals. Fig. 11 shows that the particle size of plates is increases with increasing temperature. The chemical composition of Gibbsite (aluminum hydroxide $Al(OH)_3$) is confirmed by the XRD card and SEM analysis. The chemical composition of the formed zeolite at different time and temperature is $Na_4(Al_4Si_{12}O_{32}).14H_2O$. Also, the zeolite depends on the silica and alumina ratio which represented in EDX analysis, Fig. 14.
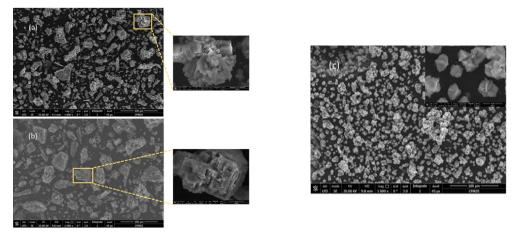

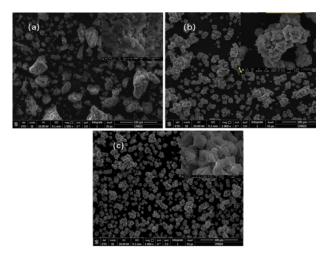Fig. 9. SEM photograph for zeolite at 100°C (a: 24 h, b: 48 h, c: 72 h)

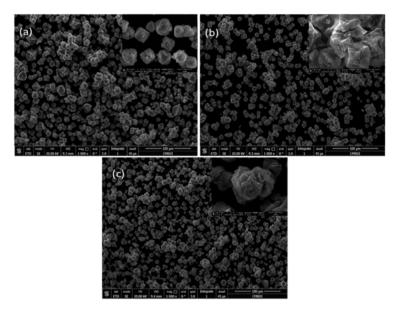Fig. 10. SEM photograph for zeolite at 120°C (a: 24 h, b: 48 h, c: 72 h)

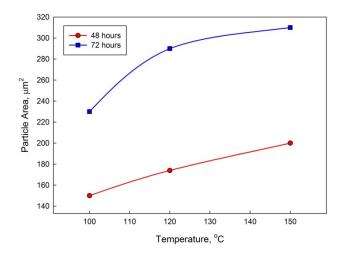Fig. 11. SEM photograph for zeolite at 150°C (a: 24 h, b: 48 h, c: 72 h)

Fig. 12. Effect of temperature on the particle area as a function of crystallization time

FTIR Spectra shows the bands near 1000 cm^{-1} are ascribed to asymmetric stretching of bonds Si-O or Al-O. These bands are close to 1000 cm^{-1} for Si-O-Al bond of the tetrahedron TO4 and confirm the presence of zeolitic material (Rodrigues et al., 2016). The symmetric stretching vibrations of zeolite NaP framework structure of Si-O and Al-O were noticed at 669 & 740 cm^{-1}. Also, the vibration band at 420 cm^{-1} region is assigned to a Si-O or Al-O bending mode. At 100°C and 24 and 48 h, the formed zeolite has gibbsite spectra with a slight decreasing in its crystalline at 48 h. A remarkable change is occurring at 72 h due to the formation of zeolite NaP. At 120°C and 150°C, zeolite NaP is formed for all crystallization time, Fig. 13.

The EDX spectra images of the product are presented in Fig. 14. The EDX revealed that the Gismondine framework of zeolite (GIS) polymorphs exhibit some differences in Si/Al ratio P2 (Si/Al = 2) where the average Si/Al ratio is about 2.1±0.1. The slight increasing than the reported ratio is depending on the preparation conditions (temperature, time and raw materials type and amount). Zubowa et al., (2008) prepared NaP with 2-2.6 Si/Al ratio using chemicals in a microwave at 150°C for 5 h. Huo et al., (2013) also synthesized NaP zeolites with variable Si/Al ratios (1.9-3) from commercial reagents.

3.3. Zeolite as adsorbate

The prepared zeolite at 150°C and 72 h is employed as adsorbate for copper and nickel ions in aqueous solutions.

Fig. 13. FTIR spectra of prepared Zeolite

Fig. 14. EDX spectra and elemental composition of high silica P Zeolite at 72 h

3.3.1. Effect of pH

The pH is an important factor affecting the site activity and the behavior of heavy metal ions such as hydrolysis, complex formation, conversion to insoluble compounds (Zhang et al., 2017). Fig. 15 shows the adsorption capacity for metal ions. The initial concentration was 400 and 40 mg/l for Ni^{2+} and Cu^{2+} ions, respectively, to match the real concentrations in real waste water. Although, zeolite normally

adsorbs cations based on the size of the hydrated ions (Visa, 2016). Generally, copper has a highest adsorption capacity for zeolites due to the small hydrated ionic radius of copper ions (Covelo, 2004). The adsorbed nickel ions are much higher than that of copper ions. It may be due to the higher initial concentration of Nickel ions. The maximum sorption capacity is achieved at pH 6. In alkaline medium, the metal ions form insoluble hydroxides, which may interfere with the sorption process. In acidic medium, the H^+ ions are competing Ni^{2+} and Cu^{2+} ions (Zare et al., 2018).

3.3.2. Effect of treatment time

Fig. 15 shows that the maximum adsorption is achieved at 40 and 60 min for Cu^{2+} and Ni^{2+} ions, respectively. The higher adsorption rate is noted up to 20 min is due to the availability of a large amount of metal ions, with empty absorption sites on the zeolite surface. Even though, the adsorption site decreases with time, the adsorption depends on the amount of transported ions from the aqueous phase to the adsorption site. So, the adsorption is continued until saturation (Duan et al., 2016). The metal ions needed more time to permeate into the narrow pores, so it took a long time to get the adsorption saturation. The initial higher rate indicates that the adsorption on the external surface, and then the adsorption is occurring in inner pores. The higher adsorption amount in the first period than that of the second period proved that the higher adsorption on the external surface than that in the internal pores (Zare et al., 2016; Abdel-Khalek et al., 2017).
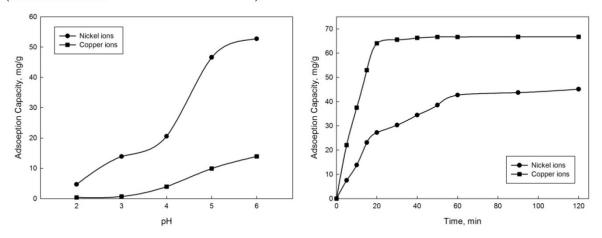

Fig. 15. Effect of pH and time on adsorption capacity of Cu^{2+} and Ni^{2+} ions

3.3.3. Adsorption kinetics

The pseudo 1st and 2nd order models are used to discuss the kinetic mechanism. These models are represented as in equations 3 and 4 (Wang et al., 2016):

For 1st order model:

$$\ln q_e - q_t = \ln q_e - K_1 t \tag{3}$$

For 2nd order model:

$$\frac{t}{q_t} = \frac{1}{K_2 q_e^2} - \frac{t}{q_e} \tag{4}$$

The q_t and q_e are the adsorbed ions (mg/g) at time t and at equilibrium. The k_1 and k_2 are the equilibrium rate constants.

Fitting of data by using both pseudo 1st and 2nd order models are shown in Fig. 16 and Table 4. On the view of the values of coefficient of determination R^2, it was evident that pseudo-second-order model was the best in describing the adsorption kinetics of heavy metal ions by zeolite. Moreover pseudo-(second-order kinetic model predicts closer values of the equilibrium adsorption capacity with the experimental values and hence it gives the applicability of this model (Abdel-Khalek et al., 2020).

The particle diffusion model is based on the chemical adsorption. It involves electron sharing or exchange between the metal ions and zeolite (Jiang et al., 2010). Adsorption may be carried out through the moving of metal ions from the aqueous phase to the surface of zeolite (Selim et al., 2020). Then the metal ions diffuse into the pores. It is usually a slow process. In most adsorption processes, the uptake

varies almost proportionately with $t^{0.5}$ rather than with the contact time and can be represented as follows (equation 5) (Covelo, 2004):
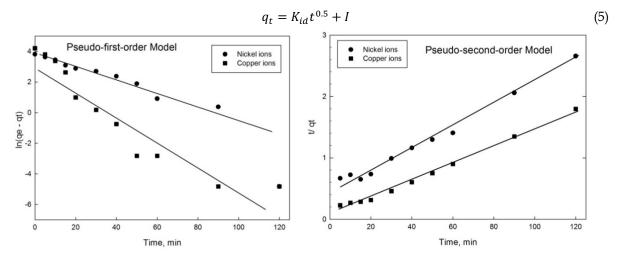
$$q_t = K_{id}t^{0.5} + I \tag{5}$$

Fig. 16. Plotting of results for pseudo-first- and pseudo-second-order models

Table 4. Calculated parameters of pseudo-first-order and pseudo-second-order models

Item	Pseudo-first-order		Pseudo-second-order	
	Nickel	Copper	Nickel	Copper
R^2	0.8841	0.8858	0.9846	0.9934
Rate constant	-0.0614	-0.0843	0.6901	0.0025
Calculated q_e	73.67	26.92	56.49	71.42
Experimental q_e	45.15	66.75	45.15	66.75

The q_t is the ions adsorbed (mg/l) at time t. The $t^{0.5}$ is the square root of the time. K_{id} (mg.g^{-1} min$^{-0.5}$) is the rate constant of intra-particle diffusion. The values of I (intercept) give information about the thickness of the boundary layer. The larger intercept means the higher effect of the boundary layer. Table 5 shows that the diffusion does not represent a limiting step in the processes on zeolite. On the other hand, the higher adsorption capacity confirming that zeolite contains mesopores, with a large number of active sites opened for the low volume cations (Mahmoud et al., 2019). However, the plot of $t^{0.5}$ against q_t, does not fit with a straight line passing through the origin but also with poor linear regression coefficients (R^2) indicating inapplicability of the model and intra-particle diffusion was not only the rate-controlling step.

Table 5. Calculated parameters of particle diffusion model

Nickel			Copper		
R^2	k_{id}	I	R^2	k_{id}	I
0.9218	4.5600	2.6614	0.962	13.183	-1.876

4. Conclusions

NaP Zeolite was prepared from aluminum and fumed silica as industrial wastes without organic template with molar ratio 1.2 at different crystallization temperature and time. A Single phase of NaP Zeolite with high crystallinity was obtained at crystallization conditions of 150°C and 72 h. The EDX analysis showed that the most appropriate ratio of SiO_2/Al_2O_3 is about 3.6. FTIR analysis assures that the final product has NaP phase. FTIR results complement the results obtained from XRD, SEM and EDX. It was found that the crystallization temperature and crystallization time are the most affecting parameters on zeolite crystallization.

The prepared zeolite could remove copper and nickel ions from aqueous solutions. At pH 6, the maximum sorption capacity is achieved at 40 and 60 min for Cu^{2+} and Ni^{2+} ions, respectively. The pseudo-second-order model described the adsorption kinetics of heavy metal ions by zeolite. It predicted closer values of the equilibrium adsorption capacity with the experimental values. The diffusion does not represent a limiting step in the processes on zeolite. The higher adsorption capacity confirming that zeolite contains mesopores, with a large number of active sites for the low volume cations.

Refe rences

ABDEL KHALEK, M.A., ABDEL RAHMAN, M.K., FRANCIS, A.A., 2017. *Exploring the adsorption behavior of cationic and anionic dyes on industrial waste shells of egg*. Journal of Environmental Chemical Engineering 5, 319-327.

ABDEL KHALEK, M.A., ABDEL RAHMAN, M.K., FRANCIS, A.A., 2020. *Experimental Design and Desirability Analysis for Optimizing the Bio-sorption of Liquid Paint-related Wastes onto Solid Eggshell Wastes*. Enviro-nmental Processes, 7, 493–508.

ABDEL KHALEK, M.A., MAHMOUD, G.A., SHOUKRY, E.M., AMIN, M., ABDULGHANY, A.H., 2019. *Adsorptive removal of nitrate ions from aqueous solution using modified biodegradable-based hydrogel*. Desalination and Water Treatment, 155, 390-401.

ADAMS, C.J., ARAYA, A., CARR, S.W., CHAPPLE, A.P., FRANKLIN, K.R., GRAHAM, P., MINIHAN, A.R., OSINGA, T.J., STUART, J.A., 1997. *Zeolite map: The new detergent zeolite*, 105 (Eds.: H. Chon, S. K. Ihm, Y. S. Uh), Elsevier ScienceBv, Amsterdam, 1667-1674.

AGUADO, J., SERRANO, D.P., ESCOLA, J.M., RODRIGUEZ, J.M., 2004. *Low temp., synthesis and properties of ZSM-5 aggregates formed by ultra-small nanocrystals*, Microporous Mesoporous Mater. 75, 41-49.

BAERLOCHER, C.H., MEIER, W.M., 1972. *Crystal structure of synthetic Zeolite Na-P1, an isotype of gismondine*. Z. Kristallogr, 135:339.

BOUKADIR, D., BETTAHAR, N., DERRICHE, Z., 2002. *Etude de la synthese des zeolites 4A et HS a partir de produitsnaturels*. In Annales de Chimie Science des Matériaux. (27), 1-13.

Cao J.L., Liu X.W., Fu R., Tan Z.Y., 2008. *Synthesis, characterization and the behavior in potassium extraction from seawater* Sep. Purif. Technol. 63, 92.

CEJKA, J., MORRIS, R.E., DAVID, D.P., 2016. *Catalysis on Zeolites*, Catal. Sci. Technol. 6, 2465-2466.

CORMA, A., 1997. *Frommicropourous to mesopours molecular sieve materials and their use in catalysis*, Chem. Rev. 97, 2373-2419.

COVELO, E.F., 2004. *Simultaneous adsorption of Cd, Cr, Cu, Ni, Pb and Zn by different soils*. J. Food Agric. Environ. 2 (3–4) 244–250.

CUNDY, C.S., COX, P.A., 2005. *The hydrothermal synthesis of zeolites: Precursors, intermediates and reaction mechanism*. Microporous Mater. 82, 1-78.

DELGADO, A.L., RODRIGUEZ, O., PADILLA, I., GALINDO, R., ANDRES, S.L., 2014. *Energy Production and Management in the 21st Century*. WIT Transactions on Ecology and The Environment, 180, 1743-3541.

DUAN, P., YAN, C., ZHOU, W., REN, D., 2016. *Development of fly ash and iron ore tailing based porous geopolymer for removal of Cu(II) from wastewater*. Ceram. Int., 42, 13507–13518.

GALINDO, R., PADILLA, I., SANCHEZ-HERNANDEZ, R., ROBLA, J.I., MONROS, G., LOPEZ-DELGADO, A., 2015a. *Production of added-value materials from a hazardous waste in the aluminum tertiary industry: Synergistic effect between hydrotalcites and glasses*. Journal of Environmental Chemical Engineering, 3, 2552-2559.

GALINDO, R., PADILLA, I., RODRIGUEZ, O., SANCHEZ-HERNANDEZ, R., LOPEZ-ANDRES, S., LOPEZ-DELGADO, A., 2015b. *Characterization of solid wastes from aluminum tertiary sector: The current state of Spanish industry*. Journal of Minerals and Materials Characterization and Engineering, 3, 55.

GARCIA, G., CARDENAS, E., CABRERA, S., HEDLUND, J., MOUZON, J., 2016. *Synthesis of zeolite Y from diatomite as silica source*. Microporous and Mesoporous Materials. 219, 29-37.

GOTTARDI, G., GALLI, E., 1985. Natural Zeolite, springer-verlag, Berlin Heidelberg, New York Tokyo, 4th ed, 14-15.

HANSEN, S., HAKANSSON, U., LANDA-CANOVAS, A.R., FALTH, L., 1993. *On the Crystal Chemistry of NaP Zeolites*, 13, 276-280.

HU, Y., LIU, X., 2003. *Composition and surface property of kaolins*. Min. Eng. 16, 1279-1284.

HUANG, Y., DONG, D., YAO, J., HE, L., HO, J., KONG, C., HILL, A.J., WANG, H., 2010. *in Situ Crystallization of Macroporous Monoliths with Hollow NaP Zeolite Structure*, Chem. Mater., 22, 5271-5278.

HUO, Z., XU, X., LV, Z., SONG, J., HE, M., LI, Z., WANG, Q., YAN, L., LI, Y., 2013. *Thermal study of NaP zeolite with different morphologies.* J. Thermal Anal. Calorim., 111, 365-369.

HUO, Z.P., XU, X.Y., LU, Z., SONG, J.Q., HE, M.Y., LI, Z.F., WANG, L.J. YAN, Q., 2012. *Synthesis, morphology control, and properties of porous metal-organic coordination polymers.* Microporous Mater. 158, 137-140.

JIANG, M.Q.; JIN, X., LU, X.Q., CHEN, Z., 2010. *Adsorption of Pb^{2+}, Cd^{2+}, Ni^{2+} and Cu^{2+} onto natural kaolinite clay.* Desalination, 252, 33–39.

LARSEN, S.C., 2007. *Nanocrystalline Zeolite & Zeolite Structures: Synthesis, Characterization & Applications.* J. Phys. Chem. C, 111, 18464-18474.

LOBO, R.F., ZONES, S.I., DAVIS, M.E., 1995. *Structure-direction in zeolite synthesis.* J. Inclusion Phenom. Mol. Recognit. Chem., 21, 47–78.

LOPEZ-DELGADO, A., ROBLA, J.I., PADILLA, I., LOPEZ-ANDRES, S., ROMERO, M., 2020. *Zero-waste process for the transformation of a hazardous aluminum waste into a raw material to obtain zeolites.* Journal of Cleaner Production. 255 (120178). ISSN 0959-6526, ESSN: 1879-1786.

LOPEZ-DELGADO, A., TAYIBI, H., 2012. *Can hazardous waste become a raw material? The case study of an aluminum residue: A review.* Waste Management and Research, 30, 474-484.

MAHINROOSTAA, M., ALLAHVERDI, A., 2018. *Hazardous aluminum dross characterization and recycling strategies: A critical review.* Journal of Environmental Management. 223, 452-468.

MAHMOUD, G.A., ABDEL KHALEK, M.A., SHOUKRY, E.M., AMIN, M., ABDULGHANY, A.H., 2019. *Removal of phosphate ions from wastewater by treated hydrogel based on chitosan,* Egyptian Journal of Chemistry, 62(8), 1537-1549.

MALONADO, M., OLEKSIAK, M.D., CHINTA, S., RIMER, J.D., 2013. *Controlling Crystal Polymorphism in Organic-Free Synthesis of Na-Zeolites.* J. Am. Chem. Soc., 135, 2641-2652.

MEFTAH, M., OUESLATI, W., CHORFI, N., AMARA, A., 2008. *Synthesis process of zeolite P using a poorly crystallized kaolinite.* Physics Procedia 00, 1081-1086.

MEIER, W.M., OLSEN, D.H., 1996. *Atlas of zeolite structure types, 4th ed., Zeolites.* Butterworth-Heinemann, London.

MOHORA, E., RONCEVIC, S., DALMACIJA, B., AGBABA, J., WASTON, M., KARLOVIC, E., DALMACIJA, M., 2012. *Removal of natural organic matter and arsenic from water by electro-coagulation/flotation continuous flow reactor.* J. Hazard. Mater. 235-236, 257-264.

MOLINER, M., REY, F., CORMA, A., 2013. *Towards the Rational Design of Efficient Organic Structure-Directing Agents for Zeolite Synthesis.* Chem. Int. Ed. 52, 13880-13889.

NAVROTSKY, A., TROFYMLUK, O., LEVCHENKO, A.A., 2009. *Phase Transitions in Meso-structured Silica/ Surfactant Composites: Surfactant Packing and the Role of Charge Density Matching.* Chem. Rev., 109, 3885–3902.

OLEKSIAK, M.D., GHORBANPOUR, A., CONATO, M.T., MCGRAIL, B.P., GRABOW, L.C., MOTKURI, R.K., RIMER, J.D., 2016. *Synthesis Strategies for Ultrastable Zeolite GIS Polymorphs as Sorbents for Selective Separations.* Chem. Eur. J. 22, 16078-16088.

OLEKSIAK, M.D., RIMER, J.D., 2014. *Synthesis oF Zeolite in the absence of organic structure directing agents: Factors governing crystal selection and polymorphism.* Rev. Chem. Eng., 30, 1-49.

RODRIGUES, M., SOUZA, A.G., SANTOS, I.M.G., 2016. *Brazilian Kaolin Wastes: Synthesis of Zeolite P at Low-Temperature.* American Chemical Science Journal. 12, 4, 1-11.

SELIM, K.A., HASAN, R., ABDEL KHALEK, M.A., YOUSEFF, M.A., ABDEL KHALEK, N.A., 2020. *Surface Modified Bentonite Mineral as a Sorbent for Pb^{2+} and Zn^{2+} Ions Removal from Aqueous Solutions.* Physico chemical Problems of Mineral Processing, 2020, 56(6), 145-157.

TSAKIRIDIS, P.E., OOUSTADAKIS, P., AGATZINI-LEONARDOU, S., 2013. *Aluminium recovery duringblack dross hydrothermal treatment.* Journal of Environmental Chemical Engineering, 1, 23-32.

VARTULI, J.C., KENNEDY, G.J., YOON, B.A., MALEK, A., 2000. *Zeolite syntheses using diamines: evidence for in situ directing agent modification.* MicroporousMesoporous Mater. 38, 247-254.

VISA, M., 2016. *Synthesis and characterization of new zeolite materials obtained from flyash for heavy metals removal in advanced wastewater treatment.* Powder Technology 294, 338-347.

WANG, N., XU X., LI H., ZHAI, J., YUAN, L., ZHANG, K., YU, H., 2016. *Preparation and application of a xanthate-modified thiourea chitosan sponge for removal of Pb^{2+} from aqueous solutions.* Ind. Eng. Chem. Res 55: 4960–4968.

XALINYUAN, 2020. http://www.xalinyuan.com/china/about.asp?ClassIDone=331 & ClassIDtwo=425, accessed on October, 8, 2020.

ZARE, E.N., LAKOURAJ, M.M., MASOUMI, M., 2018. *Efficient removal of Pb^{2+} and Cd^{2+} from water by cross-linked poly(N-vinylpyrrolidone-co-maleic anhydride) eggshell/Fe_3O_4 environ. friendly nano composite*, Desalin Water Treat 106: 209–219.

ZARE, E.N., LAKOURAJ, M.M., RAMEZANI, A., 2016. *Efficient sorption of Pb^{2+} from an aqueous solution using a poly (aniline-co-3-aminobenzoic acid)-based magnetic core–shell nanocomposite*. New J. Chem. 40, 2521.

ZHANG, H., DANG, Q., LIU, C., CHA, D., YU, Z., ZHU, W., FAN, B., 2017. *Uptake of Pb^{2+} and Cd^{2+} on chitosan microsphere surface successively grafted by methyl acrylate and diethylenetriamine*. ACS Appl Mater Interfaces 9, 11144–11155.

ZUBOWA, H.L., KOSSLICK, H., MULLER, D., RICHTER, M., WILDE, L., FRICKE, R., 2008. *Crystallization of phase pure zeolite NaP from MCM-22-type gel compositions under microwave radiation*. Microporous and Mesoporous Materials, 109, 542-548.